Genome-scale CRISPR screening in human intestinal organoids identifies drivers of TGF-β resistance

Ringel, Till ; Frey, Nina ; Ringnalda, Femke ; Janjuha, Sharan ; Cherkaoui, Sarah ; Butz, Stefan ; Srivatsa, Sumana ; Pirkl, Martin ; Russo, Giancarlo ; Villiger, Lukas ; Rogler, Gerhard ; Clevers, Hans ; Beerenwinkel, Niko ; Zamboni, Nicola ; Baubec, Tuncay ; Schwank, Gerald

Abstract: Forward genetic screens with genome-wide CRISPR libraries are powerful tools for resolving cellular circuits and signaling pathways. Applying this technology to organoids, however, has been hampered by technical limitations. Here we report improved accuracy and robustness for pooled-library CRISPR screens by capturing sgRNA integrations in single organoids, substantially reducing required cell numbers for genome-scale screening. We applied our approach to wild-type and APC mutant human intestinal organoids to identify genes involved in resistance to TGF-β-mediated growth restriction, a key process during colorectal cancer progression, and validated hits including multiple subunits of the tumor-suppressive SWI/SNF chromatin remodeling complex. Mutations within these genes require concurrent inactivation of APC to promote TGF-β resistance and attenuate TGF-β target gene transcription. Our approach can be applied to a variety of assays and organoid types to facilitate biological discovery in primary 3D tissue models.

DOI: https://doi.org/10.1016/j.stem.2020.02.007

Resource

Cell Stem Cell

Genome-Scale CRISPR Screening in Human Intestinal Organoids Identifies Drivers of TGF-β Resistance

Graphical Abstract

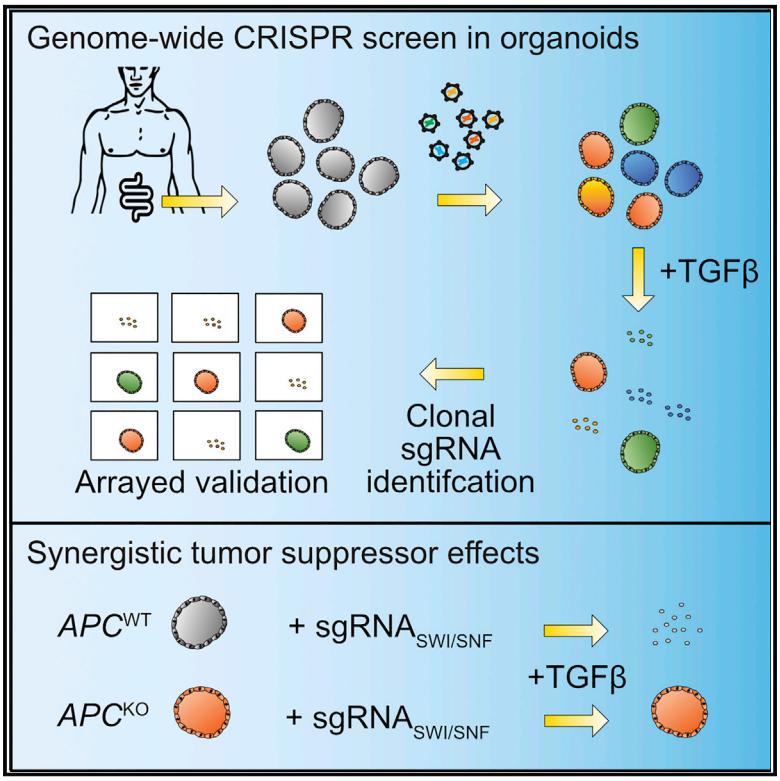

Authors

Till Ringel, Nina Frey, Femke Ringnalda, ..., Nicola Zamboni, Tuncay Baubec, Gerald Schwank

Correspondence

schwank@pharma.uzh.ch

In Brief

Ringel et al. developed a genome-wide CRISPR screening method in human intestinal organoids to dissect oncogenic signaling pathways. Several tumor suppressor genes have been identified as negative regulators of the TGF-β pathway in the context of mutant *APC*, including subunits of the SWI/SNF chromatin remodeling complex.

Highlights

- Optimized conditions enable genome-wide CRISPR screening in human intestinal organoids
- Identification of putative tumor suppressor genes that mediate TGF-β resistance
- Synergistic interactions between screening hits and *APC* regulate TGF-β response
- The SWI/SNF chromatin remodeling complex controls TGF-β target gene accessibility

Ringel et al., 2020, Cell Stem Cell *26*, 431–440
March 5, 2020
https://doi.org/10.1016/j.stem.2020.02.007

CellPress

Cell Stem Cell
Resource

Genome-Scale CRISPR Screening in Human Intestinal Organoids Identifies Drivers of TGF-β Resistance

Till Ringel,[1,2] Nina Frey,[1] Femke Ringnalda,[1] Sharan Janjuha,[1,2] Sarah Cherkaoui,[3] Stefan Butz,[4] Sumana Srivatsa,[5] Martin Pirkl,[5] Giancarlo Russo,[6] Lukas Villiger,[1] Gerhard Rogler,[7] Hans Clevers,[8,9] Niko Beerenwinkel,[5] Nicola Zamboni,[3] Tuncay Baubec,[4] and Gerald Schwank[1,2,10,*]

[1]Institute of Molecular Health Sciences, ETH Zurich, Zurich, Switzerland
[2]Department of Pharmacology and Toxicology, University of Zurich, Zurich, Switzerland
[3]Institute of Molecular Systems Biology, ETH Zurich, Zurich, Switzerland
[4]Department of Molecular Mechanisms of Disease, University of Zurich, Zurich, Switzerland
[5]Department of Biosystems Science and Engineering, ETH Zurich, Zurich, Switzerland
[6]Functional Genomics Center Zurich, University of Zurich, ETH Zurich, Zurich, Switzerland
[7]Department of Gastroenterology and Hepatology, University Hospital Zurich, Zurich, Switzerland
[8]University Medical Center (UMC) Utrecht, Utrecht, the Netherlands
[9]Hubrecht Institute, Royal Netherlands Academy of Arts and Sciences (KNAW), Utrecht, the Netherlands
[10]Lead Contact
*Correspondence: schwank@pharma.uzh.ch
https://doi.org/10.1016/j.stem.2020.02.007

SUMMARY

Forward genetic screens with genome-wide CRISPR libraries are powerful tools for resolving cellular circuits and signaling pathways. Applying this technology to organoids, however, has been hampered by technical limitations. Here we report improved accuracy and robustness for pooled-library CRISPR screens by capturing sgRNA integrations in single organoids, substantially reducing required cell numbers for genome-scale screening. We applied our approach to wild-type and APC mutant human intestinal organoids to identify genes involved in resistance to TGF-β-mediated growth restriction, a key process during colorectal cancer progression, and validated hits including multiple subunits of the tumor-suppressive SWI/SNF chromatin remodeling complex. Mutations within these genes require concurrent inactivation of APC to promote TGF-β resistance and attenuate TGF-β target gene transcription. Our approach can be applied to a variety of assays and organoid types to facilitate biological discovery in primary 3D tissue models.

INTRODUCTION

Mutations that initiate transformation of intestinal stem cells (ISCs) into cancer cells commonly occur in signaling pathways that are implicated in the communication between stem cells and their niche. Since WNT ligands play a crucial role for maintaining stemness of ISCs, it is not surprising that mutations in the *APC* gene are the most common cause for colorectal cancer (CRC) initiation (Grady and Markowitz, 2002; Moser et al., 1990). Activation of the Wnt pathway alone, however, only triggers formation of benign adenomas, and further progression into invasive carcinomas requires the accumulation of additional tumor driver mutations (Markowitz and Bertagnolli, 2009). At these later stages, inactivation of the transforming growth factor β (TGF-β) signaling pathway is frequently observed (Muzny et al., 2012). TGF-β signaling initiates growth arrest and differentiation of intestinal stem cells (Cammareri et al., 2017; Drost et al., 2015; Fessler et al., 2016), and cell-autonomous inhibition of the pathway enables cancer cells to tolerate elevated TGF-β concentrations in the CRC microenvironment (Muñoz et al., 2006; Takaku et al., 1998; Tauriello et al., 2018).

3D organoid culture systems derived from the intestine are powerful tools for modeling CRC (Drost and Clevers, 2018). While growth of organoids derived from healthy, wild-type (WT) donors are dependent on a growth factor cocktail that mimics the signaling environment of the intestinal stem cell niche, organoids established from CRC biopsies typically lose their dependency on WNT agonists, TGF-β antagonists, and EGF ligands (Figure 1A). These findings support the concept that tumor cells become gradually independent of niche signals during cancer progression and make organoids a valuable tool for studying these signaling pathways in human tissues in a physiologically relevant setting (Drost et al., 2015; Fujii et al., 2016; Matano et al., 2015).

Genome-wide CRISPR screens are routinely performed in human immortalized cell lines using pooled lentiviral sgRNA libraries (Gilbert et al., 2014; Parnas et al., 2015; Shalem et al., 2014; Wang et al., 2014). Technical limitations, however, make pooled screening analysis inherently noisy, and an approximately 500-fold library saturation is crucial for robust statistical analysis of sgRNA distributions (Canver et al., 2018; Joung et al., 2017). The resulting requirement of extensive cell numbers has hampered the application of pooled library CRISPR screening in 3D organoid cultures, and to our knowledge, only targeted screens for up to 192 genes have been reported so

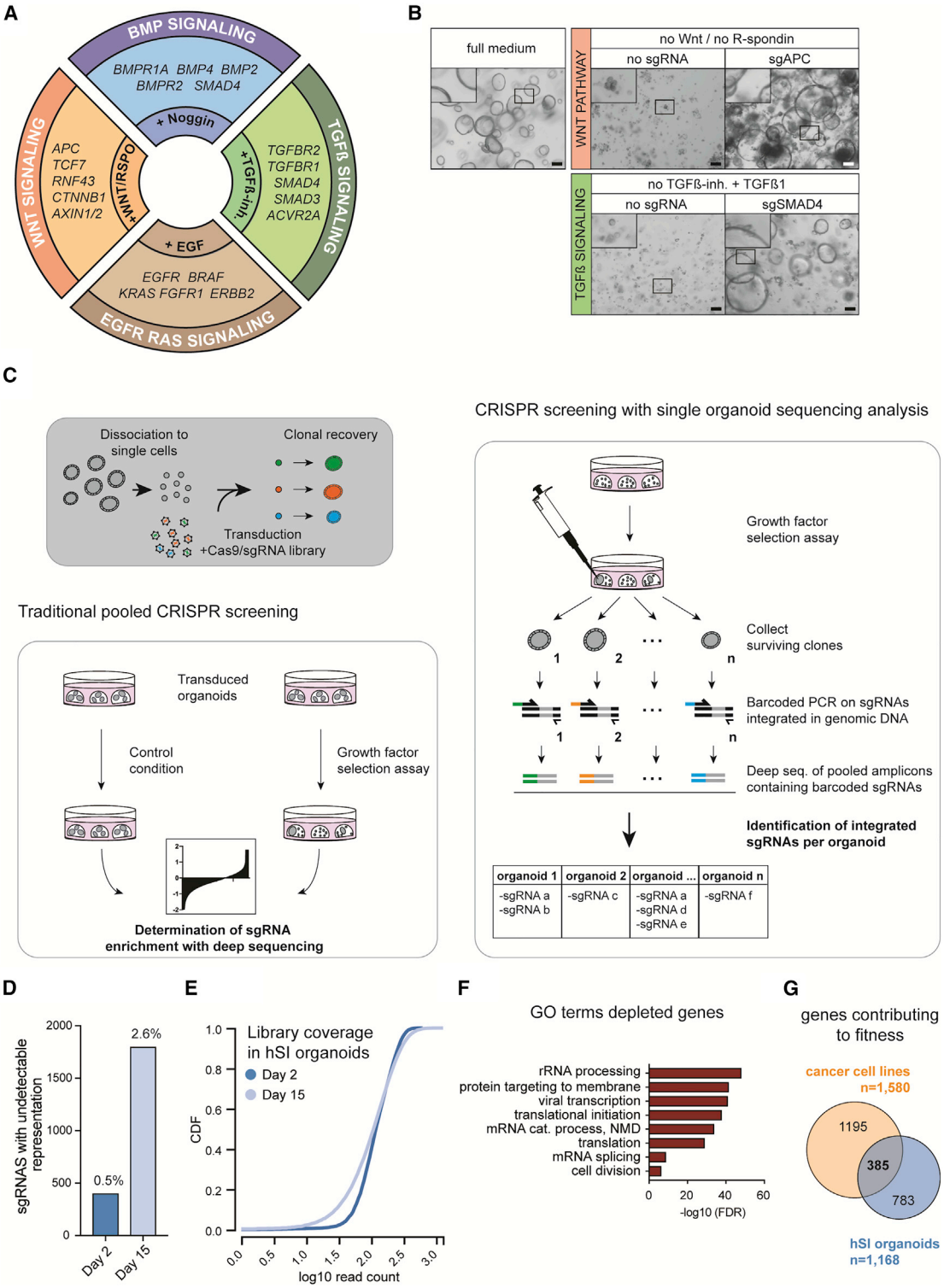

Figure 1. CRISPR Screening in Organoids with Pooled sgRNA Libraries

(A) Signaling pathways relevant for hSI organoid expansion, with supplemented growth factors (bold) and genes recurrently mutated in CRC (italic).

(B) hSI organoids cultured in full, Wnt selection, or TGF-β selection medium. Organoids were transduced with Cas9 and sgRNAs targeting *APC* or *SMAD4*. Insets show magnification of the boxed area. Scale bars 100 μm.

(C) Experimental outline for lentiviral organoid transduction (upper left), traditional pooled CRISPR screening (lower left), and pooled CRISPR screening with single organoid analysis (right). See STAR Methods for details.

(legend continued on next page)

far (Planas-Paz et al., 2019). Here, we established a method for genome-scale CRISPR screening in human small intestinal (hSI) organoids and applied it to genetically dissect the TGF-β tumor suppressor pathway.

RESULTS

Establishment of Genome-Scale CRISPR Screening in Organoids

To assess feasibility and to set up conditions for genome-wide CRISPR screening in hSI organoids, we utilized a robust assay for the Wnt pathway, where withdrawal of WNT3A and RSPO1 from the media enables selection of mutations in negative pathway regulators (Figure 1B). In a pilot screen, we applied a focused lentiviral library of 1,698 sgRNAs targeting 283 potential tumor suppressor genes (TSGs; Table S1). Transducing the library in a single organoid cell suspension of 7×10^6 cells with a MOI of 0.15 was a reasonable compromise between transduction efficiency and organoid survival (Figures S1A–S1C) and allowed us to identify the negative Wnt-regulators *AXIN1* and *APC* as hits with an FDR < 1% (Figures S1D and S1E; Table S1). However, while these results suggest that organoids can be robustly screened with targeted CRISPR libraries, we experienced that manual handling of 3D organoids makes it infeasible to obtain and transduce the cell numbers required for genome-scale screening. In addition, we observed that organoids established from single cells are growing at very heterogeneous rates, leading to a considerable distortion in sgRNA representation and hence to accessory noise in sequencing analysis. To address these challenges, we devised a screening approach where sgRNA representation is not assessed in bulk genomic DNA but captured in individual organoids (Figure 1C). Since organoids are grown clonally from single cells, this approach entirely eliminates noise generated from heterogenous growth rates. In addition, it enables direct identification of false-positive hits that originate from passenger sgRNAs co-integrated with functional sgRNAs, drastically reducing the number of genes for labor-intensive arrayed rescreening.

To test this method, we first transduced the genome-wide Brunello CRISPR library targeting 19,114 genes with each of 4 sgRNAs into an organoid single cell suspension of 7×10^6 cells and evaluated sgRNA representation by bulk genomic DNA sequencing at day 2 and day 15 after growth under permissive conditions (Doench et al., 2016). We observed a near complete library representation at day 2, which was significantly reduced at day 15 (Figures 1D, 1E, and S1F). As expected, within the group of 1,168 drop-out genes, essential processes such as translation and ribosomal biogenesis were significantly enriched, and 385 genes overlapped with core-essential genes in cancer cell lines (Figures 1F, 1G, and S1G). We next performed the Wnt pathway screen, where we transferred transduced organoids into Wnt selection conditions. Sporadically outgrowing organoids were then individually isolated, sgRNA integrations were amplified with barcoded primers, and deep sequencing with subsequent demultiplexing was used to assign sgRNAs to individual clones. A customized processing function was furthermore applied to discern clonally integrated sgRNA reads from background reads, which presumably originated from DNA traces in Matrigel co-isolated during organoid picking (see STAR Methods). Analysis of the integrated sgRNAs revealed that each organoid contained an sgRNA targeting either *APC* or *AXIN1* (Figures S2A and S2E; Table S2), demonstrating that our approach enables robust identification of functional sgRNAs from genome-wide CRISPR libraries. To our surprise, we observed that in addition to the functional sgRNA, 4 passenger sgRNAs on average were co-integrated per organoid (Figures S2A and S2E; Table S2). Since organoids grew clonally from single cells that were transduced at a MOI of 0.15, these data suggest heterogenous infection within the organoid single cell suspension.

Mutations in APC Open Additional Routes in hSI Organoids to Acquire Resistance to TGF-β

Functional analysis of CRC organoids revealed that lines not mutated in known TGF-β core pathway components are often resistant to TGF-β-mediated growth inhibition (Figure S2C) (Fujii et al., 2016), suggesting that mechanisms of TGF-β resistance in CRC are not yet fully understood. We therefore adapted our screening approach to a TGF-β selection assay, where removal of the TGF-β inhibitor and addition of the TGF-β1 ligand in the medium drives intestinal organoids into cell death (Figure 1B) (Drost et al., 2015). After transducing the genome-wide CRISPR library, cells were transferred into TGF-β selection conditions, and barcoded sgRNA amplicon sequencing was used to assign sgRNA integrations to individual organoids. Analysis of sgRNA integrations, however, revealed that the vast majority of TGF-β resistant organoids contained sgRNAs targeting known TGF-β pathway components, and only 4% of clones contained sgRNAs exclusively targeting genes without a known link to TGF-β signaling (Figure 2A; Table S2).

According to genetic models of stepwise CRC progression, mutations in the TGF-β pathway are late events and usually occur in adenoma cells, in which the Wnt pathway is constitutively activated via loss-of-function mutations in *APC* (Fearon and Vogelstein, 1990; Muzny et al., 2012). We therefore reasoned that mutations in these tumor suppressors might rely on synergistic interaction with *APC* mutations to confer resistance to TGF-β and conducted a screen in engineered *APC* mutant (APC^{KO}) hSI organoids (Figures 2B and S2B), which compared to WT organoids showed major differences in transcriptional TGF-β response (Figures 2C and 2D). Supporting our hypothesis of increased plasticity, we found that in the

(D) Bar plots showing undetected sgRNAs (less than 10 reads) after lentiviral transduction of the library. The number above the bars represents the percentage of undetectable sgRNAs from the whole library.
(E) Cumulative distribution function (CDF) of all sgRNAs after transduction in hSI organoids. The shift in the 15-day curve represents depletion of a subset of sgRNAs.
(F) Enriched GO terms among genes with depleted sgRNAs shown in (E).
(G) Venn diagram comparing depleted genes in (E) with essential genes identified in cancer cell lines (Hart et al., 2015).
See also Figure S1 and Table S1.

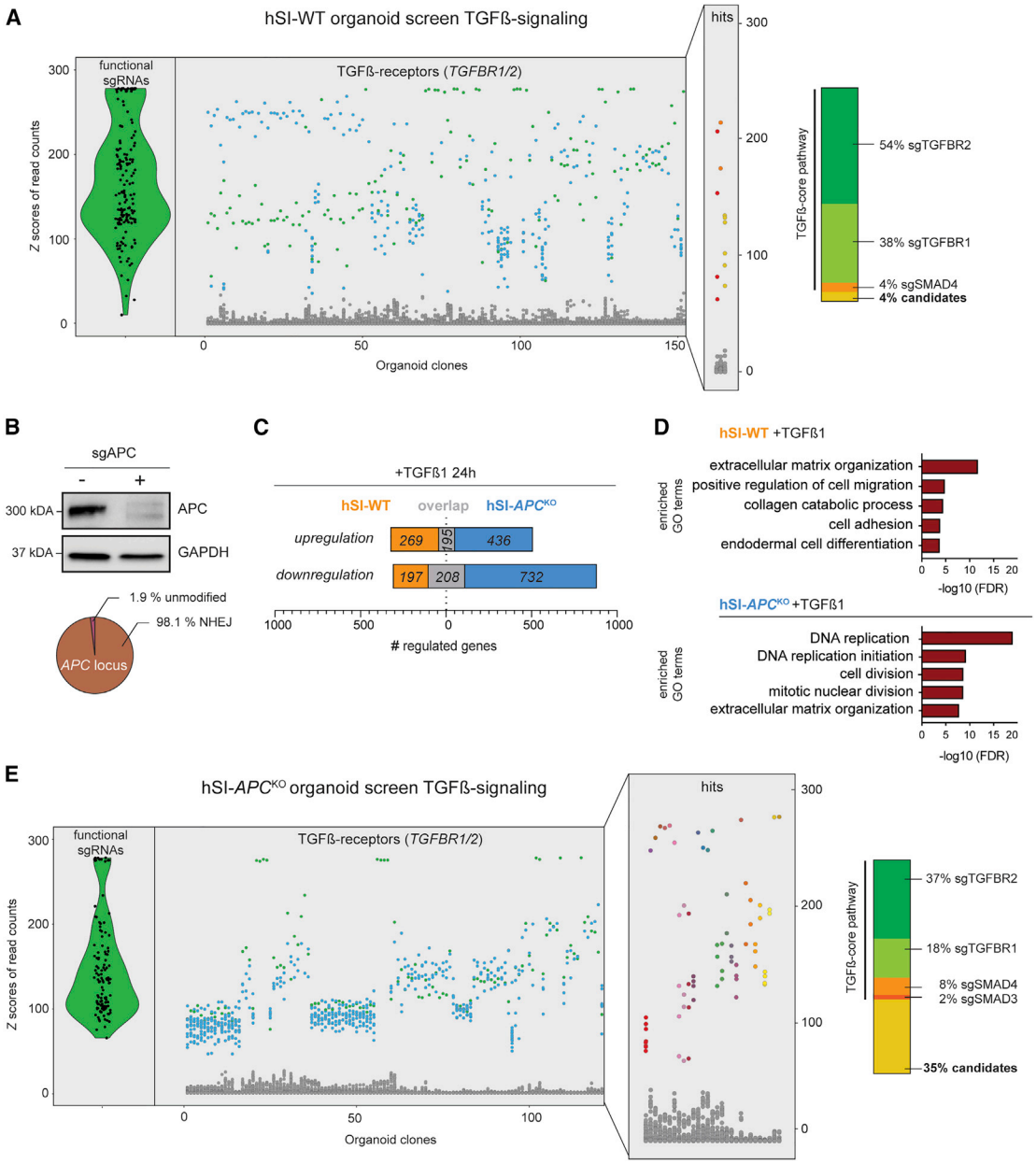

Figure 2. Single Organoid Sequencing Analysis Allows Genome-wide CRISPR-Cas9 Screening in Human Organoids

(A) Left: Dot plot showing Z-scores of sgRNAs integrated in individually recovered hSI-WT organoids from TGF-β screening. Data points for organoids with sgRNAs targeting the TGF-β core pathway are divided into passenger sgRNAs (blue) and functional sgRNAs (green). A violin plot summarizes all functional control sgRNAs targeting TGFBR1/2, and overlap with the violin plot was used as additional criteria to identify reads as integrated sgRNAs. Magnification shows organoids with sgRNAs not targeting known components of the TGF-β pathway (remaining colors). Right: Bar plots summarizing results of the WT screens. See STAR Methods for details.

(B) Confirmation of CRISPR-Cas9 generated APC mutations in hSI organoids by western blot analysis (cropped) and deep sequencing.

(C) Comparison of the transcriptional response to TGF-β in WT (orange) and APC^{KO} hSI organoids (blue). Transcriptional changes were assessed by RNA-seq. Bars show upregulated (LFC > 1) and downregulated genes (LFC < −1). Shared genes are labeled in gray.

(D) Enriched GO terms among TGF-β-induced genes in hSI-WT and hSI-APC^{KO} organoids.

(E) Dot plot showing results from TGF-β screening in hSI-APC^{KO} organoids, see (C) for explanation. n = 2 screening replicates.

See also Figure S2 and Table S2.

APC^{KO} background, 35% of organoid clones that were resistant to TGF-β did not contain sgRNAs targeting known TGF-β core-pathway components (Figure 2E; Table S2). When we next performed the TGF-β screen in organoids with an addition mutation in the tumor suppressor *TP53*, we observed that cellular plasticity was further enhanced, as organoids were occasionally

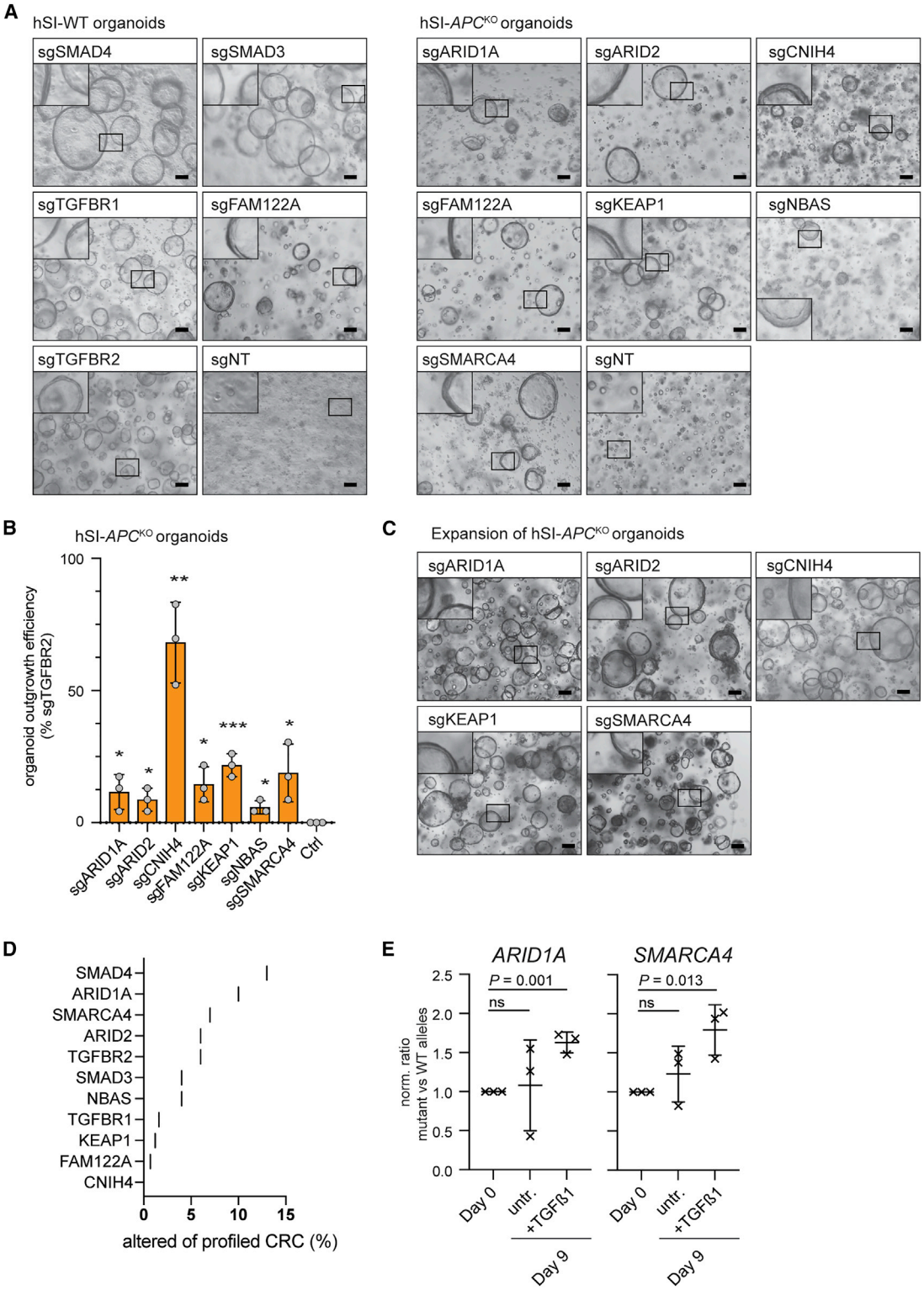

Figure 3. Validation of sgRNAs that Cause Resistance to TGF-β-Mediated Growth Inhibition in hSI Organoids

(A) hSI-WT (left) and hSI-*APC*^{KO} (right) organoids were transduced with the indicated sgRNAs identified in the WT screen and grown in TGF-β-selection-medium.

(B) Quantification of organoid outgrowth efficiency of hSI-APC^{KO} organoids in TGF-β-selection medium. Data are shown as percentage of sgTGFBR2 outgrowth efficiency. Ctrl = non-targeting sgRNA. n = 3 experiments. *p < 0.05, **p < 0.005, ***p < 0.001, Student's t test compared to control.

(C) hSI-APC^{KO} organoids transduced with indicated sgRNAs and expanded in TGF-β-selection medium over 3 passages.

(legend continued on next page)

outgrowing in the non-transduced control. Nevertheless, 19% of transduced organoids growing under TGF-β selection contained sgRNAs against TGF-β receptors, suggesting that functional hits can also be identified under less restrictive selection conditions (Figure S2D; Table S2).

Identification of Screening Hits that Confer Resistance to TGF-β in hSI Organoids

To distinguish functional hits from passenger sgRNA integrations, we performed an arrayed rescreen. We first confirmed that sgRNAs targeting the known TGF-β components *TGFBR1*, *TGFBR2*, *SMAD3*, and *SMAD4* were sufficient to confer resistance to TGF-β treatment in WT hSI organoids (Figure 3A), allowing us to dismiss all sgRNAs co-integrated in these clones for rescreening. From the screen in the WT background, we then confirmed *FAM122A* as a functional hit (Figure 3A), and from the screen in APC^{KO} organoids, we identified the two SWI/SNF components *ARID1A* and *SMARCA4* and the genes *CNIH4*, *KEAP1*, and *NBAS* as functional hits (Figures 3A and 3B). Organoids mutant for *ARID1A*, *SMARCA4*, *KEAP1*, and *CNIH4* could also be expanded under TGF-β selection over prolonged periods (Figure 3C; >4 weeks tested), and with the exception of *KEAP1* all hits could be validated by alternative sgRNAs (Figure S3A). In contrast to mutations in known TGF-β core components, which also induced resistance to TGF-β treatment in WT organoids, we found that mutations in *ARID1A*, *SMARCA4*, *CNIH4*, *KEAP1*, and *NBAS* only confer TGF-β resistance in combination with mutant *APC*. We already observed occasional outgrowth of non-transduced organoids under TGF-β selection in the APC^{KO}/$TP53^{KO}$ screen and therefore included only sgRNAs that repeatedly occurred in independent clones for arrayed rescreening. With this approach we identified an additional component of the SWI/SNF complex, namely *ARID2*, as a functional hit (Figures 3A–3C and S3A).

In summary, we identified ten genes that confer resistance to TGF-β-mediated growth inhibition in intestinal organoids when mutated, including known TGF-β pathway components and genes that have previously not been linked to TGF-β signaling (Table S2). Of note, when we performed a traditional genome-wide CRISPR screen in APC^{KO} organoids with bulk sgRNA sequencing, we only identified *TGFBR2* as a hit (Figure S3B; Table S1), confirming enhanced accuracy and robustness of the single organoid analysis approach for pooled library screening in 3D culture systems.

The SWI/SNF Components ARID1A, SMARCA4, and ARID2 Are Tumor Driver Genes in CRC

Most gastrointestinal cancers in humans develop in the colon, prompting us to test if genes identified in the hSI organoid screen also confer resistance to TGF-β-mediated growth restriction when mutated in colon organoids. We found that sgRNAs targeting *FAM122A*, *CNIH4*, *NBAS*, and the SWI/SNF subunits *ARID1A* and *SMARCA4* enabled APC^{KO} colon organoids to grow under TGF-β selection (Figures S3C–S3E). To next assess if these genes also play a role in cancer progression in patients, we used cBioportal to profile mutation frequencies across 969 CRC samples (Cerami et al., 2012; Gao et al., 2013; Giannakis et al., 2016; Muzny et al., 2012; Seshagiri et al., 2012). Notably, the group of SWI/SNF subunits (*ARID1A*, *ARID2*, and *SMARCA4*) was mutated in 18% of CRC patients, which is comparable to the mutation rate of TGF-β core-pathway components (Figure 3D). In addition, they all scored as high-confidence CRC driver genes when analyzed by the 20/20+ tumor driver prediction tool (Figure S3F) and showed strong tendencies for mutual exclusivity to *SMAD4* (Figure S3G). In line with these data, mutating *ARID1A* and *SMARCA4* in human $APC^{KO}/P53^{KO}/KRAS^{G12V}$ intestinal organoids, or *Arid2* in murine $Kras^{G12D}/Apc^{KO}$ intestinal organoids, enhanced formation of tumor nodules after xenotransplantation (Figure S3H and S3I) (Takeda et al., 2019).

To next explore if perturbation of SWI/SNF subunits confers a growth advantage to adenomas exclusively in a TGF-β-rich environment, we performed an *in vitro* competition assay where SWI/SNF mutant and SWI/SNF-WT APC^{KO} organoids were mixed in equal amounts and grown with and without the TGF-β selection, respectively. Deep sequencing of the respective WT and KO alleles confirmed that only in a TGF-β-rich environment do SWI/SNF mutant organoids have a significant growth advantage over SWI/SNF-WT organoids (Figures 3E and S3J).

Inactivation of ARID1A and SMARCA4 Modulates Transcriptional Response to TGF-β

We next investigated how mutations in SWI/SNF components could trigger resistance to TGF-β. In response to TGF-β1 binding, TGF-β receptors phosphorylate SMAD2/3, which subsequently form a stable heterodimer with SMAD4 that translocates into the nucleus and regulates target gene transcription (Dennler et al., 1998; Shi and Massagué, 2003). We therefore used SMAD2 phosphorylation as a readout to assess whether mutations in the SWI/SNF components *ARID1A* and *SMARCA4* attenuate the transduction of the signal from the TGF-β receptor to the SMAD complex. While we did not observe SMAD2 phosphorylation after TGF-β treatment in $APC^{KO}/TGFBR2^{KO}$ organoids), induction of phosphorylation in $APC^{KO}/ARID1A^{KO}$ and $APC^{KO}/SMARCA4^{KO}$ organoids was comparable to WT and APC^{KO} controls (Figure 4A), demonstrating that signal transduction upstream of the SMAD transcription factors remains functional. To next examine if the activated SMAD complex is still able to translocate into the nucleus and regulate target gene transcription, we performed RNA-seq analysis in organoids of the different genotypes before and after TGF-β treatment. Of the 1,571 differentially expressed genes in the APC^{KO} background (>2-fold, $p < 0.05$; Figures 4B and 4C), 443 were dependent on *ARID1A* or *SMARCA4* (Figures 4B and 4C). Together, these data suggest that the TGF-β-SMAD-signaling cascade is still functional in SWI/SNF mutant organoids, but the transcriptional response of TGF-β-target genes is widely attenuated.

(D) Mutation frequencies of genes identified in the screen in CRC patients. Data from 3 CRC sequencing studies with a total of 969 samples were included (Giannakis et al., 2016; Muzny et al., 2012; Seshagiri et al., 2012).

(E) Plots showing results from growth competition between $ARID1A^{WT}$ versus $ARID1A^{KO}$ and $SMARCA4^{WT}$ versus $SMARCA4^{KO}$ organoids. n = 3 experiments. Student's t test. Error bars represent SD.

Insets show magnification of the boxed area. All scale bars are 100 μm, error bars represent SD. See also Figure S3.

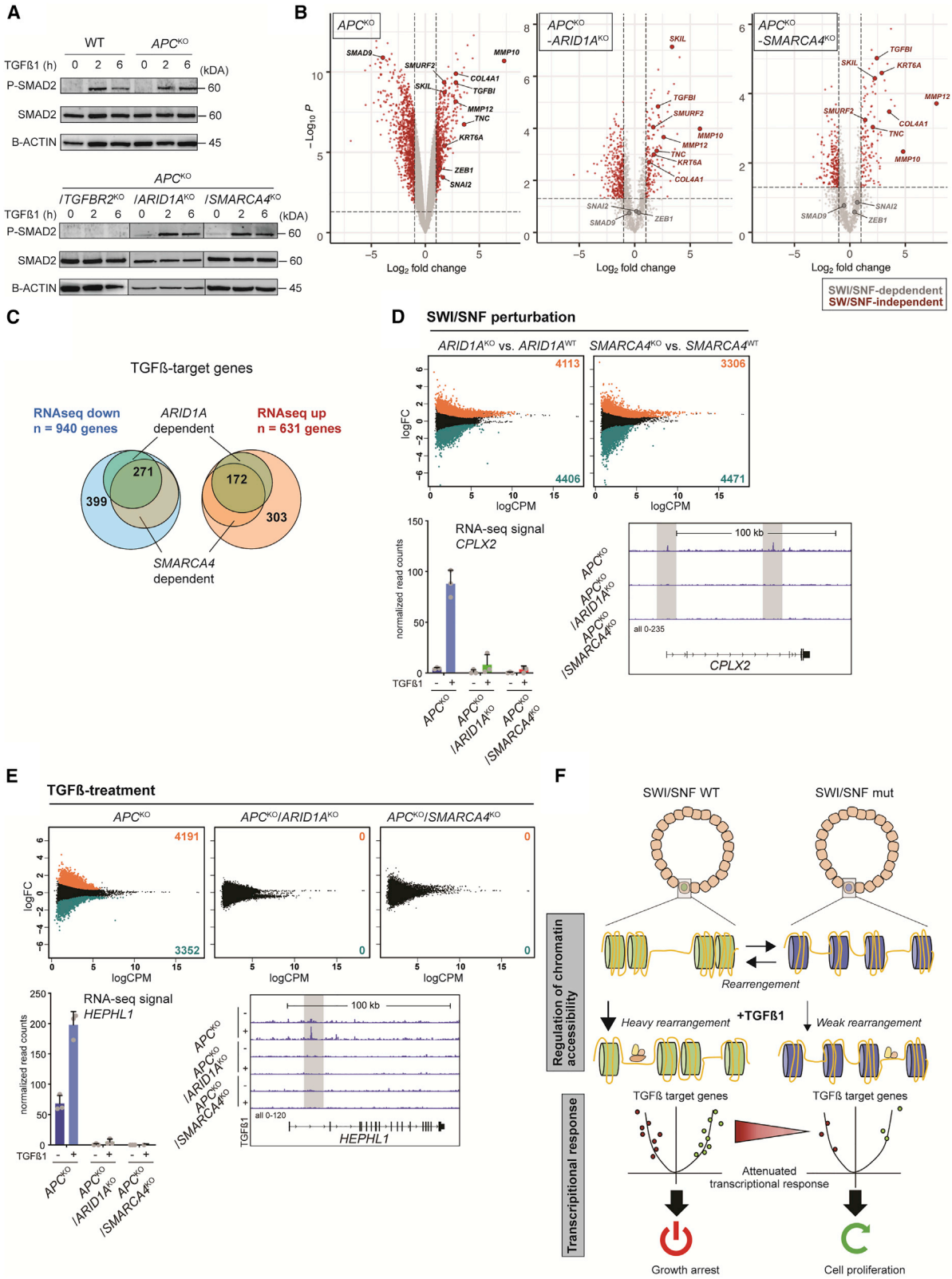

(legend on next page)

SWI/SNF-Dependent Chromatin Remodeling Is Required for Correct TGF-β Target Gene Regulation

We next aimed to unravel the underlying mechanisms of the attenuated TGF-β target gene response. Notably, mutations in SWI/SNF lead to striking changes in gene expression in hSI organoids and CRC tumors (Figures S4A and S4B). We therefore assessed whether inactivating *ARID1A* or *SMARCA4* in *APC*^{KO} organoids already leads to alterations in chromatin accessibility prior to TGF-β treatment. Performing ATAC-seq, we observed 8,819 and 7,777 sites with altered accessibility upon *ARID1A* or *SMARCA4* mutation, respectively (Figures 4D and S4C). When we specifically looked at changes in chromatin accessibility in 443 SWI/SNF-dependent TGF-β target genes, we found 61 sites with reduced accessibility (Figures 4D and S4D; Table S3). Thus, in a subset of TGF-β target genes, such as *CPLX2*, SWI/SNF perturbation might alter the chromatin conformation already prior to TGF-β pathway activation, thereby hindering proper induction of target genes (Figure 4D).

It has previously been demonstrated that SMARCA4 physically interacts with SMAD2/3, suggesting that upon recruitment to TGF-β target genes the SW/SNF complex could modulate transcriptional regulation through remodeling of nearby chromatin (Ross et al., 2006; Xi et al., 2008). We therefore next compared ATAC-seq profiles of organoids before and after TGF-β treatment. In *APC*^{KO} organoids, we found broad alterations in chromatin accessibility across the genome after treatment, which were completely absent in *ARID1A* or *SMARCA4* mutant organoids (Figure 4E). When we looked at the 443 SWI/SNF-dependent TGF-β target genes, we found that in 146 genes, such as *HEPHL1*, TGF-β-induced chromatin changes were abolished in SWI/SNF-deficient organoids, which could explain alterations in gene expression (Figures 4E and S4D). Hence, to induce a complete transcriptional response upon TGF-β treatment that results in growth inhibition in hSI organoids, SWI/SNF-dependent chromatin remodeling seems to be required.

Changes in chromatin accessibility upon SWI/SNF inactivation could attenuate TGF-β target gene response by altering DNA binding specificities of SMAD complexes. We therefore applied CUT&RUN, a method that maps protein binding on the genome, to analyze SMAD3 binding. As SMAD3 is already present in the nucleus without TGF-β pathway activation (Figure S4E) (Liu et al., 2016), we first compared SMAD3 binding between *APC*^{KO}, *APC*^{KO}/*ARID1A*^{KO}, and *APC*^{KO}/*SMARCA4*^{KO} organoids prior to treatment. Our analysis revealed that SMAD3 binding was largely altered across the genome, with only 24.5% and 23.4% of SMAD3 binding sites in *APC*^{KO} organoids being conserved in the *ARID1A* and *SMARCA4* mutant background, respectively (Figure S4F). Similarly, only a small fraction of the 3,739 TGF-β-induced SMAD3 binding sites in *APC*^{KO} organoids remained conserved in *ARID1A* and *SMARCA4* mutant organoids (1.1% and 1.7%) (Figure S4G), whereas chromatin accessibility generally remained unaltered at these sites after TGF-β (Figure S4H).

DISCUSSION

Here we established an approach for genome-wide CRISPR screening in hSI organoids. We screened for resistance mechanisms to the tumor-suppressive effects of TGF-β and identified several components of the SWI/SNF chromatin remodeling complex. Further molecular analysis led us to suggest a model where SWI/SNF modulates TGF-β target gene response via different mechanisms. While SWI/SNF could be required to prime some TGF-β target genes for transcriptional regulation, other target genes might require SWI/SNF-chromatin remodeling for pathway activation (Figure 4F). In addition, it is also conceivable that the broad transcriptomic changes upon SWI/SNF perturbation affect expression of SMAD cofactors, thereby indirectly altering TGF-β target gene regulation (Feng and Derynck, 2005; Massagué et al., 2005). The here-presented screening method would be broadly applicable to various organoid models and selection assays and could therefore open new avenues for genetically dissecting human disease mechanisms in physiologically relevant model systems.

STAR★METHODS

Detailed methods are provided in the online version of this paper and include the following:

- KEY RESOURCES TABLE
- LEAD CONTACT AND MATERIALS AVAILABILITY
- EXPERIMENTAL MODEL AND SUBJECT DETAILS
  - Human material for organoid culture
  - Mice
- METHOD DETAILS
  - Human Small Intestinal and human Colon Organoids
  - Targeted gene knock-out in organoids using lentiviral transduction
  - Lentivirus Production
  - Pooled traditional CRISPR screens
  - Library coverage and depletion assay

Figure 4. Inactivation of *ARID1A* and *SMARCA4* Alters the Transcriptional Response to TGF-β

(A) Western blot analysis of SMAD2 phosphorylation in the indicated organoid lines (cropped representative images from n = 3 experiments).

(B) Volcano plots showing transcriptional TGF-β-response in hSI-*APC*^{KO}, hSI-*APC*^{KO}-*ARID1A*^{KO}, and hSI-*APC*^{KO}-*SMARCA4*^{KO} organoids. Highlighted are examples for SWI/SNF-dependent and SWI/SNF-independent TGF-β target genes. DE genes in red: $|LFC| > 1$, $p < 0.05$.

(C) Venn diagram for genes differentially expressed upon TGF-β-treatment in hSI-*APC*^{KO}, with dependency for either *ARID1A* or *SMARCA4* (TGF-β-response mut v. WT > 50% reduced).

(D and E) Changes in chromatin accessibility in *APC*^{KO} organoids upon *ARID1A* or *SMARCA4* inactivation (D) or TGF-β treatment (E). Top panels: MA plots showing LFC of chromosome-accessibility peaks and average counts per million (CPM) of ATAC-seq analysis between *ARID1A* or *SMARCA4* inactivation (D) or TGF-β treatment (E). Bottom left panels: RNA-seq analysis for an example for SWI/SNF-dependent TGF-β-target genes *CPLX2* (D) or *HEPHL1* (E) in *APC*^{KO}, *APC*^{KO}/*ARID1A*^{KO}, and *APC*^{KO}/*SMARCA4*^{KO} organoids, with (+) or without (–) TGF-β-treatment. Bottom right: ATAC-seq analysis of *CPLX2* (D) or *HEPHL1* (E) with a gray box indicating changed chromatin accessibility in the mutant backgrounds. Error bars represent SD.

(F) Model of how SWI/SNF inactivation causes resistance to TGF-β-mediated growth repression.

See also Figure S4 and Table S3.

- Genome-wide screening using single organoid sequencing analysis
- Library saturation in screens
- Candidate validation and outgrowth quantification
- Organoid Transplantations
- Histology
- Whole mount immunofluorescence
- Western Blotting
- Generation of TSG sub library, library amplification, and cloning of individual sgRNAs
- Fluorescence-activated cell sorting (FACS)
- RNA-Sequencing
- ATAC-seq
- CUT&RUN - *chromatin profiling*
- Identification of sgRNAs in TGF-β screens
- *In-silico* tumor driver analysis
- Assessment of trends in DE genes between the transcriptomes of tumor samples and organoids

- QUANTIFICATION AND STATISTICAL ANALYSIS
- DATA AND CODE AVAILABILITY

SUPPLEMENTAL INFORMATION

Supplemental Information can be found online at https://doi.org/10.1016/j.stem.2020.02.007.

ACKNOWLEDGMENTS

We thank J. Huotari, S. Ringer, M. Jovanovic, and T. Beyer for discussions and input on the manuscript; J. Schueler and D. Lenhard for their help with performing transplantation experiments; and K. Meier and N. Gampp for their experimental support. This work was funded by the SNSF (160230). T.R. holds a PhD scholarship from ETH Zurich. L.V. holds an MD/PhD scholarship from the SNSF.

AUTHOR CONTRIBUTIONS

Conceptualization, T.R. and G.S.; Methodology, T.R., N.F., and G.S.; Software, S.C.; Formal Analysis, S.J., N.F., S.C., S.S., M.P., N.B., T.B., S.B., and G. Russo; Investigation, T.R., N.F., F.R., S.B., and L.V.; Resources, G. Rogler and H.C.; Data Curation, T.R., S.J., and G. Russo; Writing – Original Draft, T.R. and G.S.; Writing – Review & Editing, T.R., G.S., N.F., and S.J.; Project Administration, T.R. and G.S.

DECLARATION OF INTERESTS

H.C. is an inventor on applications/patents related to organoid technology. The other authors declare no competing interests.

Received: October 22, 2018
Revised: July 30, 2019
Accepted: February 13, 2020
Published: March 5, 2020

REFERENCES

Bolger, A.M., Lohse, M., and Usadel, B. (2014). Trimmomatic: a flexible trimmer for Illumina sequence data. Bioinformatics *30*, 2114–2120.

Buenrostro, J.D., Giresi, P.G., Zaba, L.C., Chang, H.Y., and Greenleaf, W.J. (2013). Transposition of native chromatin for fast and sensitive epigenomic profiling of open chromatin, DNA-binding proteins and nucleosome position. Nat. Methods *10*, 1213–1218.

Cammareri, P., Vincent, D.F., Hodder, M.C., Ridgway, R.A., Murgia, C., Nobis, M., Campbell, A.D., Varga, J., Huels, D.J., Subramani, C., et al. (2017). TGFβ pathway limits dedifferentiation following WNT and MAPK pathway activation to suppress intestinal tumourigenesis. Cell Death Differ. *24*, 1681–1693.

Canver, M.C., Haeussler, M., Bauer, D.E., Orkin, S.H., Sanjana, N.E., Shalem, O., Yuan, G.-C., Zhang, F., Concordet, J.-P., and Pinello, L. (2018). Integrated design, execution, and analysis of arrayed and pooled CRISPR genome-editing experiments. Nat Protoc. *13*, 946–986.

Cerami, E., Gao, J., Dogrusoz, U., Gross, B.E., Sumer, S.O., Aksoy, B.A., Jacobsen, A., Byrne, C.J., Heuer, M.L., Larsson, E., et al. (2012). The cBio cancer genomics portal: an open platform for exploring multidimensional cancer genomics data. Cancer Discov. *2*, 401–404.

Colaprico, A., Silva, T.C., Olsen, C., Garofano, L., Cava, C., Garolini, D., Sabedot, T.S., Malta, T.M., Pagnotta, S.M., Castiglioni, I., et al. (2016). TCGAbiolinks: an R/Bioconductor package for integrative analysis of TCGA data. Nucleic Acids Res. *44*, e71.

Constantinescu, S., Szczurek, E., Mohammadi, P., Rahnenführer, J., and Beerenwinkel, N. (2016). TiMEx: a waiting time model for mutually exclusive cancer alterations. Bioinformatics *32*, 968–975.

Davoli, T., Xu, A.W., Mengwasser, K.E., Sack, L.M., Yoon, J.C., Park, P.J., and Elledge, S.J. (2013). Cumulative haploinsufficiency and triplosensitivity drive aneuploidy patterns and shape the cancer genome. Cell *155*, 948–962.

Dennler, S., Itoh, S., Vivien, D., ten Dijke, P., Huet, S., and Gauthier, J.M. (1998). Direct binding of Smad3 and Smad4 to critical TGF beta-inducible elements in the promoter of human plasminogen activator inhibitor-type 1 gene. EMBO J. *17*, 3091–3100.

Dobin, A., Davis, C.A., Schlesinger, F., Drenkow, J., Zaleski, C., Jha, S., Batut, P., Chaisson, M., and Gingeras, T.R. (2013). STAR: ultrafast universal RNA-seq aligner. Bioinformatics *29*, 15–21.

Doench, J.G., Fusi, N., Sullender, M., Hegde, M., Vaimberg, E.W., Donovan, K.F., Smith, I., Tothova, Z., Wilen, C., Orchard, R., et al. (2016). Optimized sgRNA design to maximize activity and minimize off-target effects of CRISPR-Cas9. Nat. Biotechnol. *34*, 184–191.

Drost, J., and Clevers, H. (2018). Organoids in cancer research. Nat. Rev. Cancer *18*, 407–418.

Drost, J., van Jaarsveld, R.H., Ponsioen, B., Zimberlin, C., van Boxtel, R., Buijs, A., Sachs, N., Overmeer, R.M., Offerhaus, G.J., Begthel, H., et al. (2015). Sequential cancer mutations in cultured human intestinal stem cells. Nature *521*, 43–47.

Fearon, E.R., and Vogelstein, B. (1990). A genetic model for colorectal tumorigenesis. Cell *61*, 759–767.

Feng, X.H., and Derynck, R. (2005). Specificity and versatility in TGFb signaling through SMADS. Annu. Rev. Cell Dev. Biol. *21*, 659–693.

Fessler, E., Drost, J., van Hooff, S.R., Linnekamp, J.F., Wang, X., Jansen, M., De Sousa E Melo, F., Prasetyanti, P.R., IJspeert, J.E., Franitza, M., et al. (2016). TGFβ signaling directs serrated adenomas to the mesenchymal colorectal cancer subtype. EMBO Mol. Med. *8*, 745–760.

Fujii, M., Shimokawa, M., Date, S., Takano, A., Matano, M., Nanki, K., Ohta, Y., Toshimitsu, K., Nakazato, Y., Kawasaki, K., et al. (2016). A Colorectal Tumor Organoid Library Demonstrates Progressive Loss of Niche Factor Requirements during Tumorigenesis. Cell Stem Cell *18*, 827–838.

Gao, J., Aksoy, B.A., Dogrusoz, U., Dresdner, G., Gross, B., Sumer, S.O., Sun, Y., Jacobsen, A., Sinha, R., Larsson, E., et al. (2013). Integrative analysis of complex cancer genomics and clinical profiles using the cBioPortal. Sci. Signal. *6*, pl1.

Giannakis, M., Mu, X.J., Shukla, S.A., Qian, Z.R., Cohen, O., Nishihara, R., Bahl, S., Cao, Y., Amin-Mansour, A., Yamauchi, M., et al. (2016). Genomic Correlates of Immune-Cell Infiltrates in Colorectal Carcinoma. Cell Rep. *15*, 857–865.

Gilbert, L.A., Horlbeck, M.A., Adamson, B., Villalta, J.E., Chen, Y., Whitehead, E.H., Guimaraes, C., Panning, B., Ploegh, H.L., Bassik, M.C., et al. (2014). Genome-Scale CRISPR-Mediated Control of Gene Repression and Activation. Cell *159*, 647–661.

Grady, W.M., and Markowitz, S.D. (2002). Genetic and epigenetic alterations in colon cancer. Annu. Rev. Genomics Hum. Genet. *3*, 101–128.

Hart, T., Chandrashekhar, M., Aregger, M., Steinhart, Z., Brown, K.R., MacLeod, G., Mis, M., Zimmermann, M., Fradet-Turcotte, A., Sun, S., et al. (2015). High-Resolution CRISPR Screens reveal fitness genes and genotype-specific cancer liabilities. Cell *163*, 1515–1526.

Heinz, S., Benner, C., Spann, N., Bertolino, E., Lin, Y.C., Laslo, P., Cheng, J.X., Murre, C., Singh, H., and Glass, C.K. (2010). Simple combinations of lineage--determining transcription factors prime cis-regulatory elements required for macrophage and B cell identities. Mol. Cell *38*, 576–589.

Joung, J., Konermann, S., Gootenberg, J.S., Abudayyeh, O.O., Platt, R.J., Brigham, M.D., Sanjana, N.E., and Zhang, F. (2017). Genome-scale CRISPR-Cas9 knockout and transcriptional activation screening. Nat. Protoc. *12*, 828–863.

Langmead, B., and Salzberg, S.L. (2012). Fast gapped-read alignment with Bowtie 2. Nat. Methods *9*, 357–359.

Lawrence, M., Huber, W., Pagès, H., Aboyoun, P., Carlson, M., Gentleman, R., Morgan, M.T., and Carey, V.J. (2013). Software for computing and annotating genomic ranges. PLoS Comput. Biol. *9*, e1003118.

Li, W., Xu, H., Xiao, T., Cong, L., Love, M.I., Zhang, F., Irizarry, R.A., Liu, J.S., Brown, M., and Liu, X.S. (2014). MAGeCK enables robust identification of essential genes from genome-scale CRISPR/Cas9 knockout screens. Genome Biol. *15*, 554.

Liu, L., Liu, X., Ren, X., Tian, Y., Chen, Z., Xu, X., Du, Y., Jiang, C., Fang, Y., Liu, Z., et al. (2016). Smad2 and Smad3 have differential sensitivity in relaying TGFβ signaling and inversely regulate early lineage specification. Sci. Rep. *6*, 21602, https://doi.org/10.1038/srep21602.

Markowitz, S.D., and Bertagnolli, M.M. (2009). Molecular origins of cancer: Molecular basis of colorectal cancer. N. Engl. J. Med. *361*, 2449–2460.

Massagué, J., Seoane, J., and Wotton, D. (2005). Smad transcription factors. Genes Dev. *19*, 2783–2810.

Matano, M., Date, S., Shimokawa, M., Takano, A., Fujii, M., Ohta, Y., Watanabe, T., Kanai, T., and Sato, T. (2015). Modeling colorectal cancer using CRISPR-Cas9-mediated engineering of human intestinal organoids. Nat. Med. *21*, 256–262.

Moser, A.R., Pitot, H.C., and Dove, W.F. (1990). A dominant mutation that predisposes to multiple intestinal neoplasia in the mouse. Science *247*, 322–324.

Muñoz, N.M., Upton, M., Rojas, A., Washington, M.K., Lin, L., Chytil, A., Sozmen, E.G., Madison, B.B., Pozzi, A., Moon, R.T., et al. (2006). Transforming growth factor beta receptor type II inactivation induces the malignant transformation of intestinal neoplasms initiated by Apc mutation. Cancer Res. *66*, 9837–9844.

Muzny, D.M., Bainbridge, M.N., Chang, K., Dinh, H.H., Drummond, J.A., Fowler, G., Kovar, C.L., Lewis, L.R., Morgan, M.B., Newsham, I.F., et al.; Cancer Genome Atlas Network (2012). Comprehensive molecular characterization of human colon and rectal cancer. Nature *487*, 330–337.

Parnas, O., Jovanovic, M., Eisenhaure, T.M.M., Herbst, R.H.H., Dixit, A., Ye, C.J.J., Przybylski, D., Platt, R.J.J., Tirosh, I., Sanjana, N.E.E., et al. (2015). A Genome-wide CRISPR Screen in Primary Immune Cells to Dissect Regulatory Networks. Cell *162*, 675–686.

Pinello, L., Canver, M.C., Hoban, M.D., Orkin, S.H., Kohn, D.B., Bauer, D.E., and Yuan, G.-C. (2016). Analyzing CRISPR genome-editing experiments with CRISPResso. Nat. Biotechnol. *34*, 695–697.

Planas-Paz, L., Sun, T., Pikiolek, M., Cochran, N.R., Bergling, S., Orsini, V., Yang, Z., Sigoillot, F., Jetzer, J., Syed, M., et al. (2019). YAP, but Not RSPO-LGR4/5, Signaling in Biliary Epithelial Cells Promotes a Ductular Reaction in Response to Liver Injury. Cell Stem Cell *25*, 39–53.e10.

R Core Team. (2017). R: A Language and Environment for Statistical Computing (R Foundation for Statistical Computing).

Robinson, M.D., McCarthy, D.J., and Smyth, G.K. (2010). edgeR: a Bioconductor package for differential expression analysis of digital gene expression data. Bioinformatics *26*, 139–140.

Ross, S., Cheung, E., Petrakis, T.G., Howell, M., Kraus, W.L., and Hill, C.S. (2006). Smads orchestrate specific histone modifications and chromatin remodeling to activate transcription. EMBO J. *25*, 4490–4502.

Sanjana, N.E., Shalem, O., and Zhang, F. (2014). Improved vectors and genome-wide libraries for CRISPR screening. Nat. Methods *11*, 783–784.

Sanson, K.R., Hanna, R.E., Hegde, M., Donovan, K.F., Strand, C., Sullender, M.E., Vaimberg, E.W., Goodale, A., Root, D.E., Piccioni, F., and Doench, J.G. (2018). Optimized libraries for CRISPR-Cas9 genetic screens with multiple modalities. Nat. Commun. *9*, 5416.

Sato, T., Stange, D.E., Ferrante, M., Vries, R.G.J., Van Es, J.H., Van den Brink, S., Van Houdt, W.J., Pronk, A., Van Gorp, J., Siersema, P.D., and Clevers, H. (2011). Long-term expansion of epithelial organoids from human colon, adenoma, adenocarcinoma, and Barrett's epithelium. Gastroenterology *141*, 1762–1772.

Seshagiri, S., Stawiski, E.W., Durinck, S., Modrusan, Z., Storm, E.E., Conboy, C.B., Chaudhuri, S., Guan, Y., Janakiraman, V., Jaiswal, B.S., et al. (2012). Recurrent R-spondin fusions in colon cancer. Nature *488*, 660–664.

Shalem, O., Sanjana, N.E., Hartenian, E., Shi, X., Scott, D.A., Mikkelsen, T.S., Heckl, D., Ebert, B.L., Root, D.E., Doench, J.G., et al. (2014). Genome-Scale CRISPR-Cas9 Knockout Screening in Human Cells. Science *343*, 84–87.

Shi, Y., and Massagué, J. (2003). Mechanisms of TGF-β signaling from cell membrane to the nucleus. Cell *113*, 685–700.

Skene, P.J., Henikoff, J.G., and Henikoff, S. (2018). Targeted in situ genome-wide profiling with high efficiency for low cell numbers. Nat. Protoc. *13*, 1006–1019.

Takaku, K., Oshima, M., Miyoshi, H., Matsui, M., Seldin, M.F., and Taketo, M.M. (1998). Intestinal tumorigenesis in compound mutant mice of both Dpc4 (Smad4) and Apc genes. Cell *92*, 645–656.

Takeda, H., Kataoka, S., Nakayama, M., Ali, M.A.E., Oshima, H., Yamamoto, D., Park, J.W., Takegami, Y., An, T., Jenkins, N.A., et al. (2019). CRISPR-Cas9-mediated gene knockout in intestinal tumor organoids provides functional validation for colorectal cancer driver genes. Proc. Natl. Acad. Sci. USA *116*, 15635–15644.

Tauriello, D.V.F., Palomo-Ponce, S., Stork, D., Berenguer-Llergo, A., Badia-Ramentol, J., Iglesias, M., Sevillano, M., Ibiza, S., Cañellas, A., Hernando-Momblona, X., et al. (2018). TGFβ drives immune evasion in genetically reconstituted colon cancer metastasis. Nature *554*, 538–543.

Tokheim, C.J., Papadopoulos, N., Kinzler, K.W., Vogelstein, B., and Karchin, R. (2016). Evaluating the evaluation of cancer driver genes. Proc. Natl. Acad. Sci. USA *113*, 14330–14335.

Wang, T., Wei, J.J., Sabatini, D.M., and Lander, E.S. (2014). Genetic screens in human cells using the CRISPR-Cas9 system. Science *343*, 80–84.

Xi, Q., He, W., Zhang, X.H.-F., Le, H.V., and Massagué, J. (2008). Genome-wide impact of the BRG1 SWI/SNF chromatin remodeler on the transforming growth factor β transcriptional program. J. Biol. Chem. *283*, 1146–1155.

Zhang, Y., Liu, T., Meyer, C.A., Eeckhoute, J., Johnson, D.S., Bernstein, B.E., Nusbaum, C., Myers, R.M., Brown, M., Li, W., and Liu, X.S. (2008). Model-based analysis of ChIP-Seq (MACS). Genome Biol. *9*, R137.

STAR★METHODS

KEY RESOURCES TABLE

REAGENT or RESOURCE	SOURCE	IDENTIFIER
Antibodies		
Mouse monoclonal anti-human-cytokeratin (CAM5.2)	Becton Dickinson	CAT# 345779; RRID: AB_10687527
Rabbit monoclonal anti-phospho-SMAD2 (138D4)	Cell Signaling Technology	CAT# 3108; RRID: AB_490941
Rabbit monoclonal anti-SMAD2 (D43B4)	Cell Signaling Technology	CAT# 5339; RRID: AB_10626777
Rabbit monoclonal anti-BETA-ACTIN (13E5)	Cell Signaling Technology	CAT# 5125; RRID: AB_2223172
Rabbit monoclonal anti-GAPDH (14C10)	Cell Signaling Technology	CAT# 2118; RRID: AB_10693448
Rabbit polyclonal anti-APC	Sigma-Aldrich	CAT# SAB4501438; RRID: AB_10762093
Rabbit polyclonal anti-SMAD3	Abcam	CAT# ab28379; RRID: AB_2192903
Goat polyclonal anti-ECAD	RnD systems	CAT# AF748; RRID: AB_355568
Donkey anti-Rabbit IgG	Thermo	CAT# A10042; RRID: AB_2534017
Donkey anti-Goat IgG	Thermo	CAT# A11055; RRID: AB_2534102
Chemicals, Peptides, and Recombinant Proteins		
Advanced DMEM/F-12	Thermo	CAT# 12634028
HEPES	Thermo	CAT# 15630-056
GlutaMax	Thermo	CAT# 35050-038
Penicillin-Streptomycin	Thermo	CAT# 15140-122
EGF	Peprotech	CAT# AF-100-15
N-Acetylcysteine	Sigma-Aldrich	CAT# A9165
Gastrin	Tocris	CAT# 3006
Nicotinamide	Sigma-Aldrich	CAT# N0636
B-27 Supplement	Thermo	CAT# 17504044
A83-01 TGFBR inhibitor	Tocris	CAT# 2939
Nutlin-3	Cayman Chemicals	CAT# 548472-68-0
ROCK inhibitor Y-27632	Sigma-Aldrich	CAT# Y0503
Matrigel	Corning	CAT# 354230
Critical Commercial Assays		
Lenti-X qRT-PCR Titration Kit	Takara	CAT# 631235
Deposited Data		
CRISPR screen	This study	GEO: GSE145185
RNA-seq data	This study	GEO: GSE145185
ATAC-seq data	This study	GEO: GSE145185
CUT&RUN-seq data	This study	GEO: GSE145185
Experimental Models: Cell Lines		
Human: HEK293T	ATCC	RRID: CVCL_0063
Experimental Models: Organisms/Strains		
Mouse: NOD.Cg-*Prkdc*^{scid} *Il2rg*^{tm1Wjl}/SzJ	Charles River	RRID: ARC:NSG
HUB043	HUB platform	HUB-02-B2-043

(*Continued on next page*)

Continued		
REAGENT or RESOURCE	SOURCE	IDENTIFIER
HUB055	HUB platform	HUB-02-B2-055
HUB044	HUB platform	HUB-02-B2-044
HUB087	HUB platform	HUB-02-B2-087
Oligonucleotides		
See Table S4 for primers for sgRNA detection	This study	N/A
See Table S4 for primers for quantification of editing events	This study	N/A
See Table S4 for oligos for sgRNAs expression constructs	This study	N/A
Recombinant DNA		
lentiCRISPR v2 plasmid	Sanjana et al., 2014	RRID: Addgene_52961
Human sgRNA library Brunello	Doench et al., 2016	RRID: Addgene_73179
TSG-sub-library	This study	N/A
Software and Algorithms		
GraphPad Prism software v8.30	GraphPad	https://www.graphpad.com/scientific-software/prism/; RRID:SCR_002798
ZEN Digital Imaging for Light Microscopy	Zeiss	https://www.zeiss.com/microscopy/en_us/products/microscope-software/zen.html; RRID:SCR_013672
FlowJo software v10.2	FlowJo, LLC	https://www.flowjo.com/solutions/flowjo; RRID:SCR_008520
RStudio	RStudio	https://www.rstudio.com/; RRID: SCR_000432
Edge R Bioconductor package	Robinson et al., 2010	http://bioconductor.org/packages/release/bioc/html/edgeR.html; RRID:SCR_012802
MAGeCK v0.5.4	Li et al., 2014	https://sourceforge.net/projects/mageck/
MACS2 v2.1.2	Zhang et al., 2008	https://github.com/taoliu/MACS; RRID:SCR_013291)
Bowtie v2.3.5.1	Langmead and Salzberg, 2012	http://bowtie-bio.sourceforge.net/bowtie2/index.shtml; RRID:SCR_005476
Picard	N/A	https://broadinstitute.github.io/picard/; RRID:SCR_006525
IGV 2.5.2	Broad Institute	https://software.broadinstitute.org/software/igv/; RRID:SCR_011793
HOMER v4.10.4	Heinz et al., 2010	http://homer.ucsd.edu/homer/; RRID:SCR_010881
CRISPRScreen processing function	This study	https://github.com/cherkaos/CRISPRScreenProcessing
CLC Genomics Workbench 8	QIAGEN	http://digitalinsights.qiagen.com/products-overview/discovery-insights-portfolio/analysis-and-visualization/qiagen-clc-genomics-workbench/

LEAD CONTACT AND MATERIALS AVAILABILITY

Further information and requests for resources and reagents should be directed to and will be fulfilled by the Lead Contact Prof. Dr. Gerald Schwank (schwank@pharma.uzh.ch). All unique reagents generated in this study are available from the Lead Contact with a completed Materials Transfer Agreement.

EXPERIMENTAL MODEL AND SUBJECT DETAILS

Human material for organoid culture

Human intestinal biopsies were obtained from the University Hospital Zürich. Written informed consent was obtained from all patients, and the study was approved by the Cantonal Ethics committee of the north-western part of Switzerland and the Cantonal Ethics Committee of the Canton Zürich. CRC organoid lines were obtained from the Hubrecht Organoid Technology (HUB) platform (https://www.hub4organoids.eu).

Mice

All animal experiments were performed in accordance with protocols approved by the Kantonales Veterinaramt Zurich in compliance with all relevant ethical regulations. Male NOD.Cg-*Prkdc*^{scid} *Il2rg*^{tm1Wjl}/SzJ (NSG) mice were obtained from Charles River Laboratories and used for transplantation studies without any other interventions. Adult *NSG* mice were housed in a pathogen-free animal facility in cages with up to five animals at the Institute of Molecular Health Sciences at ETH Zurich and kept in a temperature- and humidity-controlled room on a 12-h light–dark cycle.

METHOD DETAILS

Human Small Intestinal and human Colon Organoids

Normal human small intestinal and colon tissues were isolated from resected segments derived from patients. Isolation of intestinal crypts was described previously (Sato et al., 2011). In short, the biopsies were placed in complete chelating solution CCS (5.6 mM Na_2HPO_4, 8 mM KH_2PO_4, 96.2 mM NaCl, 1.6 mM KCl, 43.4 mM sucrose, and 54.9 mM D-sorbitol). Dithiothreitol and EDTA were added just before use to a final concentration of 0.5 mM and 2 mM, respectively. The biopsies were then incubated for 20-45 min at 4°C on a rocking plate. After incubation, tubes were shaken vigorously to liberate the crypts. Tissue fragments were allowed to settle for 1 min, and supernatant containing crypts was transferred to a new tube. One volume of FBS (Sigma) was added and crypts were spun down at 150 g for 3 min. Next, the crypts were washed twice with Advanced DMEM/F12 (GIBCO) supplemented with 10 mM HEPES, 1x Glutamax, 1% Penicillin/Streptomycin and spun down for 5 min at 150 g. Crypts were subsequently resuspended in ice-cold Matrigel GFR (Corning) and plated in 20 μl drops on pre-warmed standard tissue culture plates, polymerized for 10 min at 37°C and covered with human intestinal organoid medium containing 10 μM Y-27632 RhoKinase inhibitor (Abmole) and 100 μg/mL Primocin (Invivogen). Culture medium of Human Intestinal Organoids contained Advanced DMEM/F12 supplemented with 10 mM HEPES, 1x Glutamax, 1% Penicillin/Streptomycin, 1x N2, 1x B27 (all from GIBCO), 1.25 mM *N*-acetylcysteine (Sigma), 50% WNT3A-conditioned medium (CM), 20% RSPO1-CM 20%, 10% NOGGIN-CM (all CM produced in-house), 10 mM Nicotinamide (Sigma), 50 ng/mL human EGF (Peprotech), 10 nM Gastrin (Tocris Bioscience), 0.5 μM TGF-β type I receptor inhibitor A83-01 (Tocris Bioscience) and 10 μM p38-inhibitor SB202190 (Sigma). The same medium was used for small intestinal- and colon organoids. For mutant *APC* selection, organoids were cultured in medium lacking WNT3A-CM and RSPO1-CM. For mutant *TP53* selection, organoids were cultured in the presence of 10 μM Nutlin-3a (Sigma). Organoid lines were constantly tested for mycoplasma contamination and resulted negative.

Targeted gene knock-out in organoids using lentiviral transduction

Organoids were expanded as described before, harvested in ice-cold Advanced DMEM/F12 and pelleted by centrifugation. Organoids were dissociated to the single cell level by resuspending the cells in pre-warmed TrypLE Express Enzyme 1x (GIBCO) and incubating at 37°C with occasional vigorous vortexing for 8-12 min. The dissociation process was observed under the microscope and the enzymatic reaction was stopped using DMEM supplemented with 10% FBS and 1% Penicillin/Streptomycin. The cells were pelleted and taken up in a transduction mix containing Advanced DMEM/F12 supplemented with 10 mM HEPES, 1x Glutamax, 1x Penicillin / Streptomycin, 4 ug/mL Polybrene (Merck), 10 μM RhoKinase inhibitor and concentrated lentivirus. The transduction mix was seeded in a cell culture plate and centrifuged for 1 h at 600 g at room temperature and incubated for 3 h at 37°C. Finally, the cells were harvested, seeded in Matrigel and overlaid with expansion medium containing 10 μM RhoKinase inhibitor. To select for organoids transduced with a Puromycin cassette, medium containing 1-1.5 μg / ml Puromycin (Invivogen) was added 3 days post-transduction. To select for CRISPR/Cas9-mediated knock out events, organoids were cultured for 7 days for depletion of gene products and subsequently passaged into selection medium. Successful knock-out of the target genes was validated with deep sequencing. Target-specific primers were designed flanking the predicted sgRNA cut-sites and containing primer binding sites for Illumina TruSeq Deep sequencing primers. The respective amplicons were purified and sequenced on an Illumina MiSeq System, aiming at a minimum of 5,000 reads per locus. Sequencing reads were processed with CLC Genomics Workbench 8 and mapping of the reads and quantification of editing events was performed with CRISPResso V1.0.11 (Pinello et al., 2016).

Lentivirus Production

For virus production, HEK293T cells (ATCC, RRID: CVCL_0063) were seeded in T175 cell culture flasks in DMEM (GIBCO) supplemented with 10% FBS and 1% Penicillin/Streptomycin and grown to 70% confluency. Cells were PEI-transfected with the following transfection mix: 10.4 μg psPAX2-Plasmid, 3.5 μg pMD2.G, 13.8 μg LentiCRISPRV2 in a volume of 1000 μl Opti-MEM (GIBCO) in tube 1. In a second tube, 138 μl 1mg/mL Polyethylenimine (Polysciences) was mixed with 862 μl Opti-MEM. Both tubes were equilibrated to room temperature for 5 min, mixed, and incubated 20 min at room temperature. The cells were transduced with 1600 μl of the transduction mix. After 24 h, the medium was replaced with Opti-MEM. After 48 h, the supernatant containing the lentivirus was harvested, filtered through 0.45 μm syringe filters (Sarstedt) and concentrated by centrifugation at 20,000 g for 2 h. Titration of lentivirus was performed using the Lenti-X qRT-PCR Titration Kit (Takara). Lentivirus was stored at −80°C. Plasmids psPAX2 (Addgene #12260) and pMD2.G (Addgene #12559) were gifts from Didier Trono, Plasmid LentiCRISPRV2 (Addgene #52961) was a gift from Feng Zhang.

Pooled traditional CRISPR screens

Sublibrary screen

For the pooled traditional CRISPR screens, human small intestinal organoids were expanded, harvested, and dissociated into approximately 7 × 10^6 single cells per replicate. Cells were transduced with the lentiviral tumor suppressor gene sub-library, with a physical titer of 2,56 × 10^9 viral particles/mL, in a reaction volume of 16 ml. For each of the three replicates per Wnt pathway screen, lentiviral transduction was performed separately. Transduced organoids were seeded in Matrigel and grown in expansion medium. Three days after transduction, organoids fully recovered and approximately 6 × 10^5 cells were harvested as a library baseline control, separately to medium lacking WNT3A-CM and RSPO1-CM for the Wnt-screen. On day 21 after transduction, surviving organoids were harvested from five 6-well cell culture plates and genomic DNA was extracted. Next, the integrated sgRNAs were amplified for deep sequencing using primer pair sgRNA_region_for and sgRNA_region_rev. The amplicons were processed with the Illumina TruSeq Nano DNA Library Prep Kit and paired-end sequencing was performed on a HiSeq2500 system. Reads were processed with CLC Genomics Workbench 8 and subsequent read mapping and analysis was done using MAGeCK V0.5.4.

Genome-wide screen

For the pooled traditional genome-wide CRISPR screens, human small intestinal organoids were expanded, harvested, and dissociated into approximately 7 × 10^6 single cells per replicate. Cells were transduced with the lentiviral Brunello genome-wide library with a physical titer of 2,56 × 10^9 viral particles/mL, in a reaction volume of 16 ml. For each of the screening replicates, lentiviral transduction was performed separately. A single screen was performed for the Wnt pathway, and two TGF-β screening replicates were performed per genotype (hSI-WT, hSI-A*PC*^{KO} and hSI-A*PC*^{KO}/*TP53*^{KO}), resulting in a total of six TGF-β screening replicates. Transduced organoids were seeded in Matrigel and grown in expansion medium for one week. Organoids were then passaged to TGF-β-selection medium, and 10 days after start of selection, outgrowing organoids from both replicates were harvested separately and integrated sgRNAs were sequenced. In parallel, the same number of organoid cells were transduced with the genome-wide library and grown in full medium for 2 days, before organoids were harvested and sgRNAs were sequenced as control. Differential sgRNA representation between the two TGF-β selection condition replicates and the control condition was analyzed using MAGeCK 0.5.4.

Library coverage and depletion assay

To assess library coverage, 7 × 10^6 organoid cells were transduced similar to the genome-wide organoid screening approach. At day 2 after transduction, organoids were harvested. gDNA was isolated using the QIAamp DNA Blood Midi Kit (QIAGEN) and eluted in water. sgRNA sequences were amplified from 110 μg gDNA following the suggested protocol with slight modifications (Sanson et al., 2018), using Herculase II Fusion DNA Polymerase (Agilent) and 7.5 ug of gDNA per 100 ul PCR reaction. Deep sequencing was performed with Illumina MiSeq V3 reagents, aiming at a minimum of 100 reads per sgRNA. To test depletion of sgRNAs against essential genes, hSI organoids were again transduced similar to the genome-wide organoid screening approach, and cultured for 15 days, which included one passaging step. At day 15, a total of 150 μg gDNA was isolated and used for PCR. The MAGeCK pipeline for the identification of essential genes was used for differential analysis of mapped reads 2 days and 15 days after library transduction. sgRNAs with a LFC < -0.5 and $p < 0.05$ were considered as depleted.

Genome-wide screening using single organoid sequencing analysis

For genome-wide screening, 7x 10^6 organoid cells were transduced with the Brunello sgRNA library with a physical titer of 2,56 × 10^9 viral particles/mL, in a reaction volume of 16 ml, and cultured in expansion medium. On Day 7 post-transduction, organoids were passaged into selection conditions. Of note, occasionally organoids broke in parts and continued to grow as independent organoids, explaining why some organoids had identical combinations of passenger sgRNA integrations (in Table S2 these organoids were classified into clonal events). During the passaging procedure, all wells were kept separate to avoid complete reshuffle of transduced cells. After 1-2 weeks, cystic organoids were picked, washed in ice-cold PBS and stored in PCR-reaction tubes. Extraction of genomic DNA was performed by adding 5 μl lysis mix to each single organoid, which contained 50% v/v DirectPCR Lysis Reagent (Viagen), 1 mg/mL proteinase K (QIAGEN), and incubated for 1 h at 55°C and 45 min at 85°C. For the subsequent PCR reaction, 2 μl of sample was added. Reaction was performed using NEB High-Fidelity Master mix (New England Biolabs), with 26 cycles and the barcoded target-specific primers listed (Table S4). The resulting bands were gel-purified using the NucleoSpin Gel and PCR Clean up Kit (Macherey-Nagel). The purified products were combined in batches of 30, each containing unique barcodes. The batches were concentrated using the PCR Clean up Kit and sequenced similar to the pooled screen process. The resulting reads were processed and demultiplexed using CLC Genomics Workbench 8 and reads were mapped and quantified using MAGeCK V.0.5.4.

Library saturation in screens

In our genome-wide screens, we used a lentiviral titer that transduced ~15% of the 8 mio. organoid cells (Figure S1A). Deep sequencing of organoids selected in the Wnt- and TGF-β assays revealed that transduced organoids had on average 4-5 sgRNAs integrated (Figure S2E), possibly because lentiviral transduction is limited to a subpopulation of cells in organoids. In our screens, we therefore obtained 4 × 10^6 sgRNA integrations. The genome-wide library used in our study contained 76,441 sgRNAs, and is therefore represented approximately at a 50-fold coverage.

Candidate validation and outgrowth quantification

Organoids were Puromycin selected after transduction with the desired Cas9 and sgRNA construct, and densely grown selected organoids were then harvested from four 20μl Matrigel drops. Organoids were thoroughly dissociated using TrypLE and a flame-polished Pasteur pipette and subsequently filtered through a 40 μm cell strainer. Single cells were then plated in 20 μl Matrigel drops. Only cystic organoids in a single plane of focus were counted as outgrowing organoids, and a total of eight drops were quantified. Organoid outgrowth was reported in relation to sgTGFBR2 transduced organoids, since *TGFBR2* is one of the most potent and most upstream TGF-β signaling mediators.

Organoid Transplantations

Human intestinal organoids were transplanted subcutaneously into NOD.Cg-*Prkdc*^{scid} *Il2rg*^{tm1Wjl}/SzJ (NSG, obtained from Charles River Laboratories, RRID: ARC:NSG). Per flank, 6 × 20 μl drops of organoids were injected in 100 μl PBS:Matrigel (1:1). Organoids were collected in cold Advanced DMEM/F12 to wash off the Matrigel before they were mechanically dissociated into smaller cell clusters and injected. Per genotype, a total of 4 animals was injected. Mice were controlled bi-weekly and sacrificed 9 weeks post transplantation.

Histology

Mice were sacrificed with CO_2 before s.c. tumors were extracted, dehydrated and embedded in paraffin. Paraffin sections of subcutaneous tumors were stained with Hematoxylin/Eosin as well as with anti-Human Cytokeratin (1:100, BD Biosciences, Cam5.2, RRID: AB_10687527) to label human cells.

Whole mount immunofluorescence

Per sample, 3 × 20 μl Matrigel droplets with organoids were harvested and Matrigel was removed using Cell Recovery Solution (Corning). After washing in PBS, organoids were fixed 30 min at RT in 4% PFA. Following fixation, organoids were washed 3 x in PBS before permeabilization and blocking solution was applied (10% normal donkey serum; 0.5% Triton X-100 in PBS) in 1.5 mL Eppendorf tubes overnight at 4°C on a rocker (as for all subsequent incubations). Samples were incubated with the following primary antibodies: SMAD3 (1:100, Abcam ab28379, RRID: AB_2192903), E-Cadherin (1:500, R&D Systems, AF748, RRID: AB_355568). After three washes in PBS – 0.5% Triton X-100 (PBS-T), organoids were incubated with secondary antibodies (Donkey anti-Rabbit 568, ThermoFisher A-10042, RRID: AB_2534017 and Donkey anti-Goat 488, ThermoFisher A-11055, RRID: AB_2534102; both 1:400) and counterstained with DAPI. Organoids were washed 3 x in PBS-T and mounted with ProLong Gold (Invitrogen, P36934). Confocal Images were taken with a Leica SP8 microscope at 40X magnification.

Western Blotting

Per sample, 8 × 20 μl Matrigel droplets with organoids were harvested and Matrigel was removed using Cell Recovery Solution (Corning). Samples were lysed in RIPA buffer (50 mM Tris-HCl pH 8.0, 150 mM NaCl, 0.1% SDS, 0.5% Na-Deoxycholate, 1% IGEPAL CA-630) supplemented with PhosSTOP phosphatase inhibitors and cOmplete protease inhibitor cocktail (both Roche). Protein was quantified using standard BCA protein assay (ThermoScientific). Protein was separated on 10% SDS-PAGE gels and subsequently transferred to nitrocellulose membranes (GE Healthcare) in Towbin buffer. Membranes were blocked in 5% Bovine Serum Albumin (PAN Biotech) and incubated overnight in primary antibodies phospho-SMAD2 (1:2000; Cell Signaling Technology 138D4, RRID: AB_490941), SMAD2 (1:3000; Cell Signaling Technology D43B4, RRID: AB_10626777); β-Actin (1:5000; Cell Signaling Technology 13E5, RRID: AB_2223172) and GAPDH (1:5000; Cell Signaling Technology 14C10, RRID: AB_10693448). HRP-conjugated secondary antibody was used for detection. Protein bands were visualized with Clarity ECL Western Substrate (Bio-Rad) and a Fujifilm LAS 4000 imager.

For APC blotting, samples were loaded on 4%–15% precast polyacrylamide gels (Bio-Rad) and transferred overnight to PVDF (Bio-Rad) membranes in Towbin buffer (plus 0.025% SDS). Membranes were blocked in 5% skim-milk (Rapilait) and subsequently probed with primary antibody against APC (1:750, SAB4501438 Sigma, RRID: AB_10762093).

Generation of TSG sub library, library amplification, and cloning of individual sgRNAs

For the pooled screen, we first established a list of most frequently mutated tumor suppressor genes across various epithelial cancers, including cancer of the colon, liver, lung, pancreas, prostate, kidney, ovaries, breast, bladder, thyroid, stomach, melanoma and endometrium. We used the MutSig2CV analytical branch of the Firebrowse pipeline to collect the 30 most mutated genes from each cancer, and cross checked with TUSONExplorer to select genes with a tendency toward features common in tumor suppressor genes (Davoli et al., 2013). In cases with no tendency toward oncogenic signature or tumor suppressive signature, genes were included anyways. In the next step, we used the sgRNA-Designer platform of the Broad Institute to design 6 sgRNAs per genes, resulting in 1,698 sgRNAs against 283 genes (https://portals.broadinstitute.org/gpp/public/analysis-tools/sgRNA-design; Doench et al., 2016). Using the protocol from Shalem et al., we adapted the sgRNA design for subsequent cloning into the LentiCRISPRv2 backbone (Shalem et al., 2014). The Brunello library was ordered from Addgene (#73179). For sufficient coverage and equal sgRNA distribution across the library, the vector including the sgRNA was electroporated into Endura Electrocompetent *E. coli* (Lucigen) and plated on ten 10 cm LB agar plates (TSG) and four 24,5 cm bio assay dishes. Bacterial colonies were scraped off and plasmid DNA

was isolated using the Nucleo Bond Midi X-Plus Kit (Macherey-Nagel). Individual sgRNAs were cloned using the same protocols, but only single bacterial clones were picked for plasmid DNA isolation.

Fluorescence-activated cell sorting (FACS)

Human small intestinal organoids were transduced with a lentivirus carrying Cas9-GFP and sgRNA against *APC* and analyzed 7 days after transduction. Organoids were dissociated with TrypLE Express Enzym (GIBCO), and resuspended in FACS buffer (1% FBS, 5 mM EDTA and 10 μM RhoKinase inhibitor in PBS). Sytox Red (Invitrogen) was added for the exclusion of dead cells. Data were acquired on a BD LSR Fortessa cell analyzer (Becton Dickinson) and were further analyzed using FlowJo software (FlowJo 10.2). In all experiments, a minimum of 50,000 cells were analyzed, if not stated otherwise. For gating, forward versus side scatter (FSC-A versus SSC-A) gating was used to identify cells of interest. Doublets were excluded using the forward scatter height versus forward scatter area density plot (FSC-H versus FSC-A). Live cells were gated based on Sytox-Red-negative staining. Live-gated cells were further used to quantify the percentage of eGFP negative and eGFP positive populations.

RNA-Sequencing

Library preparation

For RNA extraction, 8 × 20 μl Matrigel droplets with organoids were harvested and organoid pellets were lysed in RLT buffer. RNA was isolated using the RNeasy Kit (QIAGEN) according to the manufacturer's instructions. The quality of the isolated RNA was determined with a Qubit® (1.0) Fluorometer (Life Technologies) and a Bioanalyzer 2100 (Agilent). Only those samples with a 260 nm/280 nm ratio between 1.8–2.1 and a 28S/18S ratio within 1.5–2 were further processed. The TruSeq RNA Sample Prep Kit v2 (Illumina) was used in the succeeding steps. Briefly, total RNA samples (100-1000 ng) were poly-A enriched and then reverse-transcribed into double-stranded cDNA. The cDNA samples were fragmented, end-repaired and polyadenylated before ligation of TruSeq adapters containing the index for multiplexing. Fragments containing TruSeq adapters on both ends were selectively enriched with PCR. The quality and quantity of the enriched libraries were validated using Qubit® (1.0) Fluorometer and the Caliper GX LabChip® GX (Caliper Life Sciences). The libraries were normalized to 10nM in Tris-Cl 10 mM, pH8.5 with 0.1% Tween 20. The TruSeq PE Cluster Kit HS4000 or TruSeq SR Cluster Kit HS4000 (Illumina) was used for cluster generation using 10 pM of pooled normalized libraries on the cBOT. Sequencing was performed on the Illumina HiSeq2000 single end 100 bp using the TruSeq SBS Kit HS4000 (Illumina, Inc, California, USA).

Data analysis

Reads were quality-checked with FastQC. Sequencing adapters were removed with Trimmomatic and reads were hard-trimmed by 5 bases at the 3′ end (Bolger et al., 2014). Successively, reads at least 20 bases long, and with an overall average phred quality score greater than 10 were aligned to the reference genome and transcriptome of *Homo sapiens* (FASTA and GTF files, respectively, downloaded from GRCh38) with STAR v2.5.1 with default settings for single end reads (Dobin et al., 2013). Distribution of the reads across genomic isoform expression was quantified using the R package GenomicRanges from Bioconductor Version 3.0 (Lawrence et al., 2013). Differentially expressed genes (DE) were identified using the R package edgeR from Bioconductor Version 3.0 (Robinson et al., 2010).

A gene is marked as DE if it possesses the following characteristics: 1) at least 10 counts in at least half of the samples in one group, 2) $p < 0.05$. and 3) log2 ratio > = 1.

ATAC-seq

Library preparation

Library preparation was carried out with minor modifications as described elsewhere (Buenrostro et al., 2013). For ATAC-Seq with hSI organoids, organoids were dissociated into single cells and 50,000 cells were lysed in 50 μl cold Lysis buffer (10 mM Tris-HCl, pH 7.4, 10 mM NaCl, 3 mM MgCl2, 0.1% IGEPAL CA-630). After centrifugation at 500 g for 10 min at 4°C, cells were resuspended in 1X transposition mix (Illumina; 25 μl Tagment DNA Buffer, 2.5 μl Tagment DNA Enzyme, 22.5 μl ddH_2O) and incubated for 30 min at 37°C on a shaker at 300 rpm. Immediately after the transposition reaction, DNA was purified using the QIAgen MinElute PCR Purification Kit according to the manufacturer's instructions. Library was amplified with Nextera Sequencing primers in NEBNext Q5 Hot Start HiFi 2X PCR master mix for 5 cycles. To remove large DNA fragments, the PCR reaction was incubated with 0.55X AMPure XP beads (Beckman Coulter) and the unbound supernatant was subsequently purified with QIAgen MinElute coloumns. Again, DNA was amplified with Nextera Sequencing primers in NEBNext Q5 Hot Start HiFi 2X PCR master mix for 9 cycles. Finally, to remove primers and small DNA fragments, PCR reaction was bead-purified with 1.8X AMPure XP beads. Bound DNA was eluted in 20 μl EB buffer and quantified and visualized for quality control with a 2200 TapeStation System (Agilent).

Data processing

Raw sequencing reads were filtered for low-quality after adaptor removal and aligned on GRCh38 using Bowtie2 with default mapping parameters (Langmead and Salzberg, 2012). PCR duplicates were removed using Picard. The mapped reads of all replicates were merged for each condition prior to peak calling. Peaks were called on each sample using MACS2 with "–nomodel–shift −100–extsize 200," to obtain a consensus peak set for each sample (Zhang et al., 2008). The peak set was used to build a count matrix using the aligned reads for all samples and their replicates. Differential peaks between sample groups were identified using edgeR. For this, the count matrix was filtered for peaks with low coverage across all samples based on minimum read count of 10 for each sample. The remaining counts were normalized using the total library size as well as edgeR's TMM derived normalization

factors. Between two sample groups, only regions with a log fold change above > 0.5 and an FDR value < 0.05 were considered as differentially accessible for further analysis. The peaks were annotated using HOMER (Heinz et al., 2010).

CUT&RUN - *chromatin profiling*

Library preparation

Cut and Run targeted chromatin profiling was performed as described by Skene et al. (Skene et al., 2018). In brief, for each condition, 200.000 single cells were harvested from human small intestinal organoids. After two washes, cells were bound to 10 μl of Concanavalin A-coated beads (Bangs Laboratories, cat. no. BP531), diluted in 1ml of binding buffer and rotated 10 min at RT. Cells were cleared on a magnetic rack and beads were resuspended in 50 μl antibody solution. The antibody anti-SMAD3 (1:50, abcam28379; RRID: AB_2192903) was used, and incubated on a rotator overnight at 4°C. Beads were cleared on a magnetic rack and washed in digitonin buffer before resuspension in 50 μl of digitonin buffer with 700 ng/μl pA-MNase (kindly received from Kopf/Henikoff Lab), in order to bind the fusion protein to the antibody. After 1h rotating at 4°C, beads were cleared on a magnetic rack and washed twice. To activate MNase activity, beads were resuspended in 150 μl digitonin buffer and chilled down to 0°C before 3 μl of 100 mM $CaCl_2$ were added for 30 min at 0°C. Reaction was stopped by adding 150 μl of 2X Stop buffer and tubes were incubated for 10 min at 37°C to release chromatin. After centrifugation for 5 min at 4°C at 16 000 g, tubes were placed on a magnetic rack in order to remove beads. The supernatant was collected and purified using the NucleoSpin PCR clean up kit (Macherey-Nagel, cat. no. 740609.250). DNA was stored at −20°C before Illumina library preparation.

Sequencing libraries were made using the NEBNext® Ultra II DNA Library Prep Kit for Illumina (E7645) according to the manufacturer's description. Clean up steps between the reactions (End repair/Adaptor ligation and PCR) were performed by using AMPure XP beads (Beckmann Coutler, A63881). Quality control of amplified libraries was carried out on an Agilent 2200 TapeStation System and Paired-End Sequencing was performed on an Illumina NovaSeq Machine.

Data processing

Quality control of fastq files was done using FastQC before analysis was started. After adaptor and PCR duplicate removal reads were mapped to the human genome (GRCh38) using Bowtie2 with options "–local–very-sensitive-local–no-unal–no-mixed–no-discordant–phred33 -I 10 -X 700." Differential peaks in SMAD3 binding (Treated versus Untreated) were called using MACS2, applying the following parameters: "–nomodal–extsize 160." Profiles were displayed using IGV version 2.5.3. The peaks were annotated using HOMER.

To consider a peak as overlapping between the ATAC-Seq dataset and SMAD3 CUT&RUN dataset, the center of the ATAC-Seq peak should lie between the start and end coordinates of a SMAD3 peak.

Identification of sgRNAs in TGF-β screens

To identify sgRNAs for follow up experiments, we have devised a processing function in R (R Core Team, 2017). Because of the nature of our screening approach, in which we do not compare treated and non-treated pools, we decided to use the information of abundant positive controls to identify functional sgRNAs. We first selected positive control clones with high read counts for sgRNAs targeting known positive regulators (APC, AXIN, TGFBR1/2). For these control clones, we identified integrated sgRNAs, removed background sgRNAs reads, and applied the learned pattern to analyze integrated sgRNAs in clones. Processing function steps:

1. Manual identification of positive control organoid clones with high read counts for sgRNAs targeting known positive regulators.
2. For all integrations, Z-scores of the reads are calculated to make read count values comparable to each other.
3. For each control clone, the processing function ranks sgRNAs from high to low and identifies largest drop in read count (fold change) between two consecutive sgRNAs.
4. The smallest read count drop (fold change) among control clones is selected as minimum threshold for integrated sgRNAs.
5. Identification of sgRNAs in non-control clones: only clones with sgRNAs read count drop bigger than the threshold are selected by processing function.
6. Generation of summary table containing control clones and non-control clones (candidates) with identified integrated sgRNAs. Data available in Table S2.

In-silico tumor driver analysis

Prediction of driver genes was performed using 20/20+ version 1.0.3 with the in-built trained classifier and parameters "NUMSIMULATIONS: 100000" and "NUMITER: 10" (Tokheim et al., 2016). For the mutations, we combined the MAF files for colorectal adenocarcinoma from TCGA (Giannakis et al., 2016; Seshagiri et al., 2012).

In order to test for mutual exclusivity between the screening hits and members of TGF-β pathway, we used TiMEx version 0.99.0 (Constantinescu et al., 2016). We focused only on TCGA samples as we used both mutations and copy number alterations in the input binary alterations matrix, and reported the resulting significant ($q < 0.1$) interactions.

Assessment of trends in DE genes between the transcriptomes of tumor samples and organoids

We used the R package 'TCGABiolinks' (Colaprico et al., 2016) to access RNaseq data and mutation profiles for the colorectal adenocarcinoma (COAD) dataset. We collected data from patients with no mutations in the TGF-β core pathway (Smads, receptors) and defined three subgroups: 1) The control group not possessing mutations in SWI/SNF components, 2) the first SWI/SNF-perturbed group consisting of patients with a mutation in *SMARCA4*, and 3) the second SWI/SNF-perturbed group consisting of patients

with a mutation in *ARID1A*. We performed a differential expression analysis between the control and each perturbed group using the R package 'edgeR'. To compare the transcriptional changes, we looked at the overlap of the LFC-ranked lists as a function of the top n genes. To assess significance of the overlap, we used a permutation test. We randomly permuted the ranks of the lists and again computed the overlap as a function of the top n genes as before. The permutation was performed 10,000 times. We considered as significant an overlap above the 5%-significance level, i.e., an overlap larger than 95% of all permutations.

QUANTIFICATION AND STATISTICAL ANALYSIS

Data are presented as mean of *N* biological replicates and with standard deviation (SD). Exact value of *n* is stated in the figure legends. No strategy for experiment randomization was used, and no blinding was used in the study. No samples or animals were excluded from the analysis.

Significance of data was analyzed using the two-tailed, unpaired *Student's t test* function in Prism (GraphPad) for the comparison of two groups.

The MAGeCK package (https://sourceforge.net/projects/mageck/, v.0.5.4) was used to analyze pooled CRISPR screen outcomes. Total read counts were chosen as normalization method, and $p < 0.05$ was chosen as a cut off for significantly enriched or depleted genes.

DATA AND CODE AVAILABILITY

Results of sequencing of pooled screens are provided in Table S1. Results of single organoid sequencing are provided in Table S2. Results of chromatin accessibility profiling and profiling of transcription factor binding are provided in Table S3.

The datasets generated during this study are available at Gene Expression Omnibus (GEO). Original DNA-sequencing data for Figures 1 and 2, source RNA sequencing data for Figures 2 and 4, ATAC-seq and CUT&RUN data for Figure 4 are deposited under accession number GEO: GSE145185.